

## Robotic-Assisted 3D Scanning and Laser Thermography for Crack Inspection on Complex Components

by P. D. Hirsch\*, S. K. Kunji Purayil\*, J. Lecompañon\*, N. W. Pech-May\*\* and M. Ziegler\*

\* Bundesanstalt für Materialforschung und -prüfung (BAM), Unter den Eichen 87, 12205 Berlin, Germany, philipp-daniel.hirsch@bam.de

\*\* Manufacturing Metrology Team, Faculty of Engineering, University of Nottingham, Advanced Manufacturing Bldg., 522 Derby Rd, Lenton, Nottingham NG7 2GX, United Kingdom

### Abstract

The integration of automation and robotics into non-destructive testing (NDT) marks a significant advancement in evaluating complex components. This paper introduces a novel approach using robotic-assisted laser thermography combined with automated 3D scanning to detect and analyze cracks in complex structures. The system uses an integrated line scanner with a robotic arm to capture high-resolution data, creating detailed 3D models for adaptive path planning and precise alignment correction. Laser thermography, based on localized heating and the "flying spot" approach, detects surface-near cracks with high precision. Crack detection is achieved using the Canny algorithm optional on Fourier-transformed thermograms, offering robust results with minimal computation. This study highlights the potential of robotic-assisted 3D scanning and laser thermography as efficient and precise methods for crack inspection, advancing NDT technologies and ensuring the structural integrity of modern components.

### 1. Introduction

The integration of automation and robotics into inspection processes has fundamentally transformed the evaluation of complex components. This study introduces an innovative approach utilizing robot-assisted laser thermography for the automated identification and detailed analysis of cracks in intricate structures through scanning laser thermography. This method not only streamlines the inspection process but also eliminates numerous manual steps and the use of chemicals required in traditional methods such as dye penetrant inspection. Given the increasing complexity of components, especially in additively manufactured parts, this is a crucial step towards ensuring component safety over a long lifecycle.

The proposed workflow enables users to measure complex components without the need for an exact digital copy. Due to significant wear and tear or the handcrafted nature of many carbon fiber reinforced polymer (CFRP) parts, there are substantial differences between ideal models and actual components. In small batch production, the traditional workflow for robot-assisted inspections poses challenges in ensuring traceable fixturing with suitable reference surfaces, as designing appropriate fixtures can be time-consuming and expensive. The presented approach aims to minimize these hurdles in the inspection of complex components, allowing inspectors to conduct examinations efficiently. Additionally, the path planning tool is precisely tailored to the needs of the optical inspection method of active laser thermography, allowing for the selection and consideration of a focus area.

### 2. Methodology

#### 2.1. Calibration methods

Before the system can be used, all components must be calibrated. Typically, most robotic tools require multiple learned points to calibrate a tool or object. A common practice is to move sharpened rods towards each other to define points. Optical inspection systems complicate this process. Additionally, the thermographic test setup in our laboratory is subject to regular changes.

#### 2.2. Laser line scanner

The primary function of the sensor is to measure the components. Its positional accuracy in space is crucial for the quality of the measurement results. Calibration is fully automated using a reference target, minimizing 12 degrees of freedom. The laser line sensor's position and attitude can be described by three translational movements: along the laser line ( $x_{\text{laser}}$ ), in the beam direction ( $z_{\text{laser}}$ ), and perpendicular to it ( $y_{\text{laser}}$ ). It also requires knowledge of its rotation around each axis:  $\alpha_{\text{laser}}$ ,  $\beta_{\text{laser}}$ ,  $\gamma_{\text{laser}}$ . For the calibration target, the horizontal lower edge is defined as  $x_{\text{target}}$ , the vertical edge as  $y_{\text{target}}$  and the forward direction as  $z_{\text{target}}$ , as illustrated in figure 1.



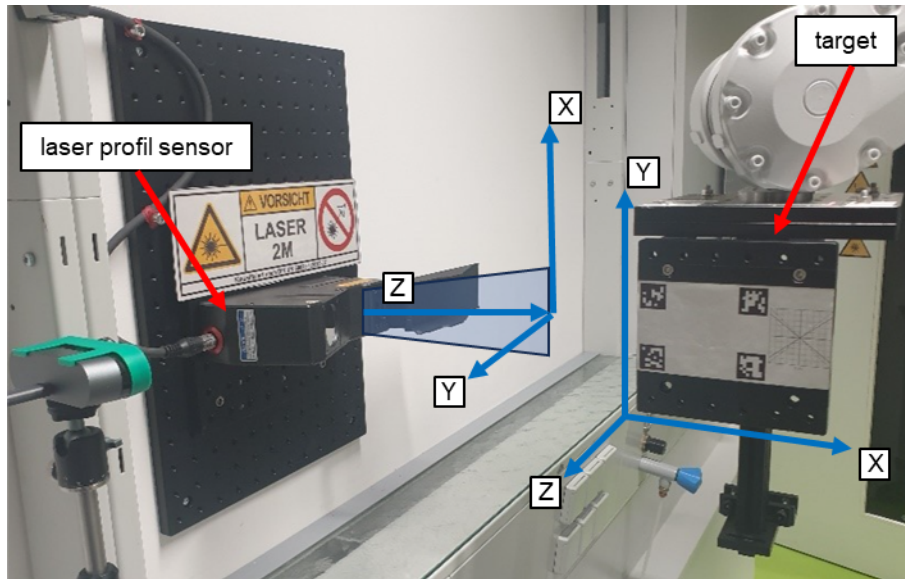


**Fig. 1.** Laser scanner (left) with calibration target (right) and their corresponding coordinate systems

A TCP/IP interface was established to control the robot, allowing it to move and alter the definitions of the tool (the laser line sensor) and the work object (the calibration target) using a custom-designed protocol.

The target only needs to be roughly manually calibrated with a precision of a few millimeters. Subsequently, the calibration target is moved in front of the laser line sensor, and its output is recorded. In the first measurement, the distance and angle between the sensor and the target are determined from one side and then from the opposite side. Given the known size of the target,  $z_{\text{laser}}$ ,  $\beta_{\text{laser}}$ ,  $x_{\text{target}}$  and  $\gamma_{\text{target}}$  can be determined. In the next step, a horizontal laser line measurement is performed on the lower and then the upper part of the target's front side. The tilt of the laser line corresponds to the rotation around the y-axis of the target ( $\beta_{\text{target}}$ ), and the angle calculated from the movement path and distance change corresponds to the rotation of the target around the x-axis ( $\alpha_{\text{target}}$ ). The sensor's measured distance ( $z_{\text{laser}}$ ) is already inherently calibrated, allowing for correction of the  $z_{\text{target}}$  position.

Next, the target is positioned so that its lower edge faces the laser, correcting  $y_{\text{target}}$ . Then, the target is moved so that the sensor is "centered" on an edge, with measurements falling off at a  $45^\circ$  angle to the sides. Lines are fitted to these data series to interpolate the intersection, thus calculating the position of the edge. The deviation from the ideal center position is the correction for  $x_{\text{target}}$ . The described nine degrees of freedom require only single laser profiles at each point. For the last three degrees of freedom, another edge is recorded. This time this is done with the target parallel to the laser line and tilted with  $\gamma_{\text{target}} = 30^\circ$ , as the target moves in  $y_{\text{laser}}$  in front of the sensor. This is repeated with a different distance to the sensor ( $z_{\text{laser}}$ ). The recorded data is evaluated to determine when the edge was recorded, identifying  $y_{\text{laser}}$ . The angle described by the edge in the recording sequence corresponds to the sensor's rotation around z ( $\gamma_{\text{laser}}$ ). Measurements at different distances also allow the calculation of the sensor's rotation around the x-axis ( $\alpha_{\text{laser}}$ ). Some measurements are interdependent, requiring an iterative process for increasingly accurate calibration. After three iterations of this process, no significant changes can be observed anymore.

Despite the high accuracy of the robotic system, it was essential to always return to a position a few centimeters away during individual measurements to approach the target position from the same direction, minimizing the influence of backlash on the measurements.

	Translation (Euclidean Distance)		Rotation	
	Mean [mm]	Standard Deviation [mm]	Mean [°]	Standard Deviation [°]
Laser Scanner	0.047	0.018	0.28	0.12
Reference Body	0.028	0.012	0.0032	0.0016

**Table 1.** Adjustment verification result

Table 1 shows the results of a small parameter study where the work object definition was manipulated five times with random numbers (translation  $\pm 2$  mm and Rotation  $\pm 1^\circ$ ), followed by the calibration routine. The greatest challenge was accurately determining the laser's alignment.

### 2.3. Thermography setup

The setup for the laser thermography system is partially automated. The target for the adjustment, which can be mounted on the robot in almost any orientation, is the same calibration target as described and calibrated using the laser scanner calibration routine. For calibrating the infrared camera and the line of the excitation laser, a test pattern was designed, consisting of two areas. One area includes a target surface for the laser, framed by four ArUco [1] markers (a simple form of QR codes), and the second area is a checkerboard pattern with auxiliary lines for manual camera adjustment.

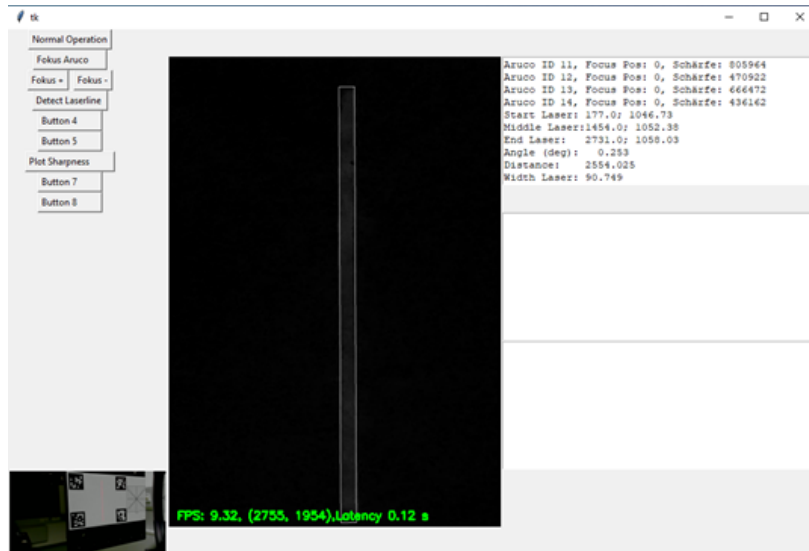


*Fig. 2. User Interface for Laser Focus Calibration*

First, the laser line is measured by irradiating the first area of the test pattern. An optical camera is used for observation and evaluation. Based on the ArUco markers, the position of the pattern in the image can be determined, and a perspective correction is performed and therefore the absolute position of the camera is not important. The program, which conducts the image evaluation, controls the robot's forward and backward movements. During this process, the camera focus is automatically adjusted, and the position and size of the laser line are calculated. The GUI is shown in figure 2. On the left-hand side are buttons to select the functions and the raw image view of the camera below. In the centre is the image of the detected laser line in black and white including a border around the line. On the right, current parameters of the script are displayed, such as the size of the laser line. All six degrees of freedom of the laser can be determined from this, and the robot's definition is adjusted accordingly. The process is repeated to verify the changes.

Next, the second part of the pattern is positioned in front of the sensor. The checkerboard pattern assists the user in manually aligning the camera to the center of the image and adjust the focus. Given the high spatial resolution of the camera ( $30\ \mu\text{m}$  to  $70\ \mu\text{m}$ , depending on the measurement scenario) and the precise adjustability of the camera mount, an alignment accuracy of less than  $0.1\ \text{mm}$  can easily be achieved. The depicted test pattern, currently made of paper, was used for the development of the procedure. A laser-engraved metal plate and one with toner applied via transfer printing are in progress.

### 2.4. 3D Laserscanner

The laser line scanner, in conjunction with the 6-axis robot, functions as a 3D scanner. This solution was chosen for several reasons:

- Full integration into the robot's coordinate system, ensuring that the generated models align with the robot's coordinate system.
- High automation potential for scanning entire components or specific sections. For instance, in a series of identical components, a quick check can be performed on a corner to see if it is misaligned.
- No reconstruction artifacts and a very high spatial resolution of  $20\ \mu\text{m}$  along the line at a working distance of  $211\ \text{mm}$  to  $279\ \text{mm}$ .

There are two methods for scanning entire components. The first method involves the user defining simple geometries, invoking functions in the ABB robot's RAPID programming language to describe a cylindrical path or rasterize a surface with different angles. This allows a scan to consist of any number of sub-measurements. A custom made application visualizes these shapes to simplify parameterization. The second method involves using a path from a path

planning program or the functions presented later. However, this requires preliminary information about the component. A two-stage approach can be beneficial here, where an initial scan is performed using simple geometries, and based on this scan, a path is generated and followed.

Once all preparations are complete, the script for recording the laser profiles and robot position data, as well as the robot script for the movement is started. The robot transmits its position data every 4 ms over the network, while the line sensor records 12 Mpx/min in operating mode. Based on the robot's position, the corresponding 3D-locations in space are subsequently calculated.

The path planning is designed to work with way points. However, if the component has undercuts, it may be advantageous to first calculate a mesh and then export a uniform point cloud. It is useful to use the Poisson algorithm to create a mesh from a point cloud using the point normals and treat the reconstruction as a problem of solving a Poisson equation, creating a coherent and closed 3D mesh that represents the underlying geometry of the point cloud. The algorithm takes into account global properties of the point cloud and often produces smoother and more complete surfaces compared to other methods [2].

## 2.5. Path planning

The planning tool was designed to work with point clouds of the external surface of components. When internal structures are included in the mesh, converted from CAD data, a specific function is employed to filter these structures. This function utilizes a Fibonacci sphere with perspective points around the component, registering all visible points to ensure accurate filtering.

Paths are generated along predefined cutting planes with an adjustable path spacing. The spacing between measurement points can be specified flexibly to accommodate various requirements. These measurement points define a path that the robot follows at a constant speed. This process involves balancing the accuracy of the described path, which benefits from densely packed points, with the need for maintaining a consistent travel speed. The actual test distance is determined by the scan speed and the frame rate of the thermal imaging camera. For instance, in the measurement presented in section 3, the distance was 0.05 mm or 0.075 mm (5 mm/s at 100 Hz, 15 mm/s at 200 Hz) with a spatial resolution of 0.069 mm/px.

For measuring the edge (tip) of the blade, a specialized function calculates a path along the center of the tip. This function is specifically designed for this purpose, ensuring precise measurements of critical areas. Additionally, a third function has been implemented, which projects a given area (determined by the movement direction and laser width) onto a segment of the component. Although this function has not yet been utilized for the current test object, it provides flexibility for future measurements [3].

A crucial point is the ability to set the focus point not simply in the middle of the path. Instead, the function examines the position of all points in the current section that are within a specified angle range ( $-45^\circ$  to  $45^\circ$ ) relative to the camera and generates a point that seeks the ideal focus point for all points. Furthermore the system offers an adjustable alignment strategy, allowing for z-rotation either perpendicular to the direction of travel or following the surface contour. This flexibility ensures optimal alignment for various measurement scenarios. Adjustable lead-in and lead-out paths, providing smooth transitions into and out of the measurement zones.

To assist users in planning and executing measurements, the tool includes a visualization feature. This feature displays the inspection path and the achieved measurement points based on the chosen setup (image height, and focus area of the laser and thermal imaging camera). This visualization aids in verifying that the planned paths and measurements will cover the necessary areas accurately and efficiently.

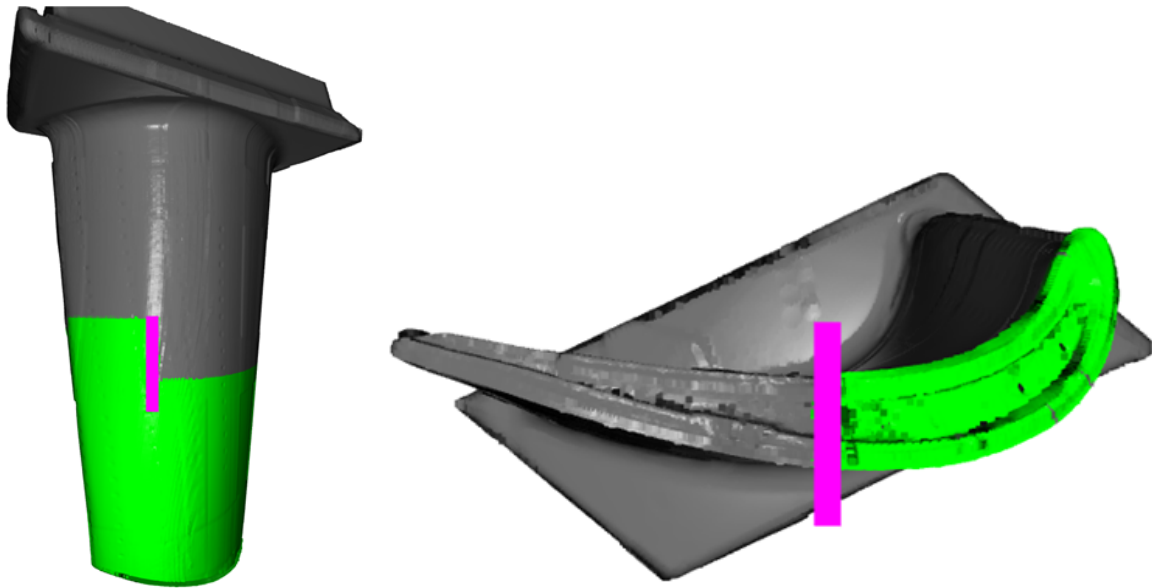


**Fig. 3.** Visualisation of the measurement run on the test specimen with green marking of the surface already recorded

Overall, this tool streamlines the process of setting up and executing detailed inspections, ensuring high precision and reliability in the measurements while providing users with the flexibility and control needed to adapt to various inspection requirements. The final step is the export to a rapid program so that the robot can follow the path independently and the movement trajectories are shown in the following figure 4.

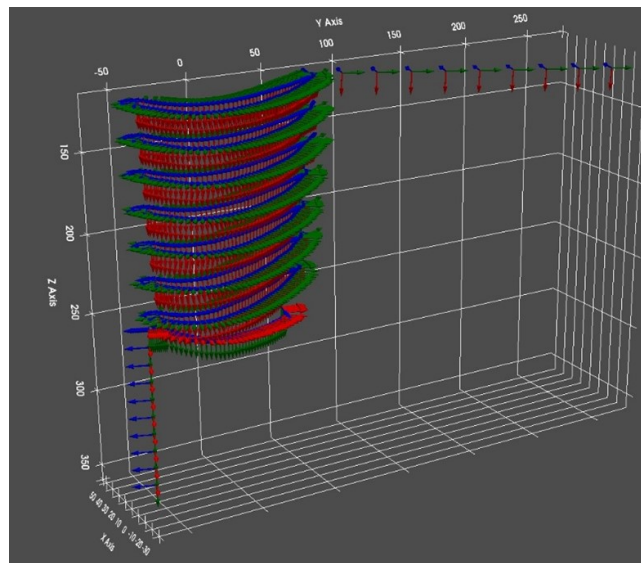


**Fig. 4.** Movement trajectory of the robot for the measurement

### 3. Thermographic testing

The focus lies in the preparation for the actual measurement. Figure 5 shows the test setup for active laser thermography for crack detection. The camera is an MWIR-camera with a resolution of  $1280 \text{ px} \times 1024 \text{ px}$  and an image frequency of 100 Hz in full frame. The excitation laser with a maximum of 500 W and a wavelength of 940 nm is deflected by means of two partially transparent mirrors. This enables the positioning of 2 cameras on-axis, i.e., with the same perspective. To synchronize the camera with the robot, a microcontroller records frame-sync signals from the camera and the robot's data packets with the positions. In post-processing, all data is fused together for every recorded image [4].

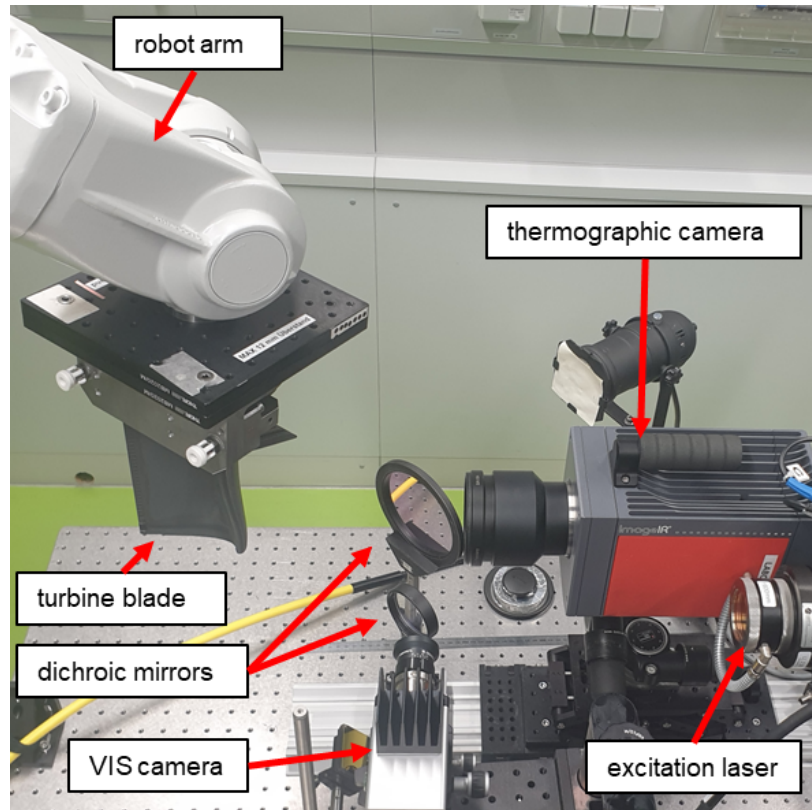


**Fig. 5.** Thermographic measurement setup

The experiments were conducted at various speeds and power settings. The slowest test was performed at a speed of 5 mm/s and, including reorientations between the paths, required 501 s for the hot gas area of inspected gas turbine blade. The laser power was set at 35 W over an area of 68 mm × 1.14 mm, corresponding to a power density of 45 W/cm<sup>2</sup> and an energy density of 8.4 J/cm<sup>2</sup>. In the stitched thermograms, such as figure 6, numerous other structures are visible in addition to the defects.

These additional structures can be attributed to varying surface roughnesses. The crack detection is based on edge detection, which captures all these surface transitions and thus leads to false positives.

For detailed information on the thermography workflow, we refer to a comprehensive description given in [4, 5, 6].

#### 4. Results and discussion

The path planning based on real surface contours has substantially improved the quality of the robot's paths. This approach ensures that the robot follows the exact geometry of the component, resulting in more accurate and reliable inspections. The requirements of optical measurement technology are better taken into account. The ability to adapt the path planning to the specific contours of each part minimizes errors and enhances the precision of the inspection process.

The custom-built portfolio of functions provides a versatile toolkit that allows for easy adaptation to various components with different inspection requirements using robotic NDT. This flexibility is crucial for addressing the diverse needs encountered in practical applications. When specific tasks require movement trajectories that closely follow the contours of a component, custom functions can be implemented to meet these unique demands. This capability ensures that the system can handle a wide range of inspection scenarios effectively.

The requirements for holding fixtures for components have drastically decreased with this system. It is now only necessary to secure the component in place without the need for precise reference surfaces for repeatable fixturing. This simplification is significant, as it reduces the preparation time and cost associated with creating custom fixtures. For instance, 3D-printed plastic holders have been successfully used to secure components. This method is both cost-effective and adaptable to different shapes and sizes of parts. If the inspection hardware (camera, laser, etc.) is mounted on the robot, the component can simply be placed on a table, further reducing the setup complexity.

The results of the presented measurement can be seen in the stitched thermogram along a predefined path shown in figure 6. There, sharp fluctuations in the measured temperatures can be recognised over the entire blade. Upon closer inspection in the section in the left figure 7, hotspots caused by cracks are visible (highlighted in blue boxes). These hotspots indicate areas where the thermal response suggests the presence of cracks, making it possible to identify and

assess potential defects accurately. Other indications in the thermogram are due to the edges of the component, which can create false positives or additional noise in the data.

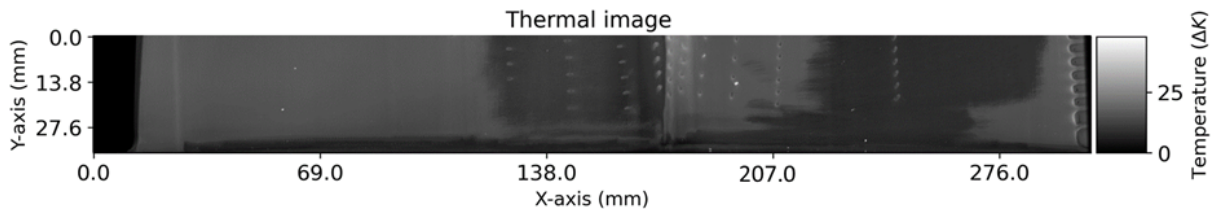


**Fig. 6.** Stitched thermogram of one slice at the turbine blade with a region of interest (red box)

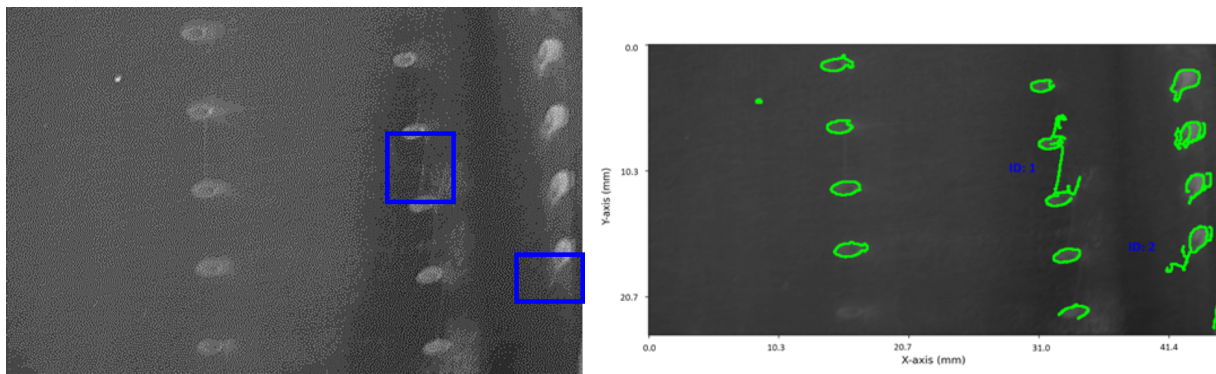


**Fig. 7.** Left: small image section with recognisable indications; right: applied edge detection with green markings

An edge detection algorithm is used to recognise the defects, which provides an image with adjacent areas marked in green. The surface of the component was quite inhomogeneous due to manual grinding, resulting in varying degrees of roughness. These variations in surface texture are visible as streaks in the thermogram, which shows how important it is to consider the surface conditions for the analysis of the data.

## 5. Conclusion

This study presents a novel approach for integrating robotic laser thermography to automate the identification and detailed analysis of cracks in complex structures. The methodology, which combines precise path planning with edge detection algorithms, enhances the accuracy and reliability of inspections. The ability to adapt path planning to specific component contours and the flexibility to create custom functions in Python for unique movement trajectories make the system versatile and suitable for various inspection scenarios. The reduction in fixture requirements, achieved through the use of 3D-printed plastic holders and the elimination of the need for precise reference surfaces, simplifies the inspection process. This reduces setup time and costs, making the system more efficient and user-friendly.

The results, illustrated by stitched thermograms, demonstrate the system's ability to detect hotspots caused by cracks. An important task now being worked on is the filtering of indications generated from component edges by taking into account surface contour and overlaying the data with the VIS camera recordings. Overall, this work advances the field of robotic non-destructive testing by leveraging robotic systems, laser thermography, and computational techniques. The developed solution addresses key challenges in inspecting complex components, improving the efficiency and accuracy of the inspection process. This approach provides a scalable and adaptable framework for future developments in automated inspection technologies.

## REFERENCES

- [1] S. Garrido-Jurado, R. Muñoz-Salinas, F. Madrid-Cuevas, and M. Marín-Jiménez. "Automatic generation and detection of highly reliable fiducial markers under occlusion". In: *Pattern Recognition* 47.6 (2014), pp. 2280–2292. DOI: <https://doi.org/10.1016/j.patcog.2014.01.005>.
- [2] M. Kazhdan, M. Bolitho, and H. Hoppe. "Poisson surface reconstruction". In: *Proceedings of the Fourth Eurographics Symposium on Geometry Processing*. SGP '06. Cagliari, Sardinia, Italy: Eurographics Association, 2006, pp. 61–70.
- [3] S. L. Arlinghaus, W. C. Arlinghaus, W. D. Drake, and J. D. Nystuen. *Practical Handbook of Curve Fitting*. Boca Raton, FL: CRC Press, 1994. URL: <http://hdl.handle.net/2027.42/58759>.
- [4] N. W. Pech-May, P. Hirsch, J. Lecompañon, and M. Ziegler. "Robot-assisted infrared thermography for surface breaking crack detection on complex shaped components". In: *SPIE Future Sensing Technologies 2023*. Ed. by O. Matoba, C. R. Valenta, and J. A. Shaw. SPIE, May 2023. DOI: 10.1117/12.2666757.
- [5] N. W. Pech-May and M. Ziegler. "Surface breaking crack detection algorithm for flying spot and line thermography based on the Canny approach". In: *SPIE Future Sensing Technologies 2021*. Ed. by M. Kimata, J. A. Shaw, and C. R. Valenta. Vol. 11914. International Society for Optics and Photonics. SPIE, 2021, p. 119140M. DOI: 10.1117/12.2603913. URL: <https://doi.org/10.1117/12.2603913>.
- [6] A. Salazar, A. Mendioroz, and A. Oleaga. "Flying spot thermography: Quantitative assessment of thermal diffusivity and crack width". In: *Journal of Applied Physics* 127.13 (Apr. 2020), p. 131101. DOI: 10.1063/1.5144972. URL: <https://doi.org/10.1063/1.5144972>.